

Boomerang flight mechanics: Unsteady effects on the motion characteristics

Original

Boomerang flight mechanics: Unsteady effects on the motion characteristics / Battipede, M.. - (1997), pp. 355-366.
(Intervento presentato al convegno 22nd Atmospheric Flight Mechanics Conference, 1997 tenutosi a usa nel 1997).

Availability:

This version is available at: 11583/2986587 since: 2024-03-06T09:55:57Z

Publisher:

American Institute of Aeronautics and Astronautics Inc, AIAA

Published

DOI:

Terms of use:

This article is made available under terms and conditions as specified in the corresponding bibliographic description in the repository

Publisher copyright

AAAS preprint/submitted version e/o post-print Author Accepted Manuscript

preprint/submitted version e/o post-print Author Accepted Manuscript

(Article begins on next page)

BOOMERANG FLIGHT MECHANICS: UNSTEADY EFFECTS ON THE MOTION CHARACTERISTICS

Manuela Battipede, Ph.D Student
Aeronautical and Space Department, Polytechnic of Turin
Turin - ITALY

Abstract. This work describes a simulation program suitable for predicting the behavior of the boomerang in function of its geometrical characteristics, of the throw parameters and of the environmental conditions, taking into account any non-stationary states corresponding to some motion steps (throw, transition from helicopter mode to autogyro mode, landing). These phases certainly have a significant effect on the characteristics of the trajectory. Boomerang has been treated as a lifting rotor and the nonlinear Pitt-Peters dynamic inflow model has been used, even at very high values of the advancing ratio. The mathematical model is strongly nonlinear and thus greatly dependent on the initial condition. The influence of different environmental conditions as well as different geometric and throw parameters have been shown through the graphical comparison of the geographical trajectories. Each qualitative trend has been experimentally verified and this is a preliminary confirmation of the reliability of the numerical code. Finally a whole flight has been described and analysed in each aspect and the necessity to use an unsteady model has been shown through a time-topographical analysis of the advancing blade angles of attack.

Introduction

The reasons of the classical two blade boomerang can be summarized in a few words: boomerang is nothing more than an eccentric-hub rotor, consisting of high-efficiency airfoils, fitted at a nearly null angle. In this statement two different concepts are contained: they are concerned with the main characteristics that a good boomerang might have to perform its typical flight.

- *Rotor autorotative ability:* autorotation is the well known regime, during which the rotor is moved by the aerodynamical forces, through a continuous extravasation of energy from potential to kinetic. In the case of the helicopter, autorotation is the phase that follows an engine fail: no longer sustained by engine power the helicopter starts to descend, thus acquiring a positive w velocity component. The resulting

local angles of attack would bring to the stall if the pilot did not accomplish the manoeuvre to enter in autorotation, which consists in a rapid reduction of the collective pitch, that is, of the airfoils incidence. The boomerang has no controls, so the only way to supply it with autorotative ability is to shape it directly with very low angles of incidence. A suited airfoil is a flat-convex one, that generally has high efficiency, thus featuring a high lift at null angle of attack. In this way the boomerang can perform its descent in the best way, with a long glide that, anyway, does not occur in autorotation regime: generally only the last tract of the trajectory is sometimes performed in a vertical autorotation regime, but boomerang can anyway greatly benefit from this property, throughout its descent.

- *Gyroscopic characteristics:* the two-blade boomerang is not quite a gyroscope, that is a rotating body with a round inertial ellipsoid, but it can always be defined as a high gyroscopical stability system. Its swept angle has just the aim of making the J_{yy} inertial moment of the same order of magnitude of J_{xx} : the boomerang gyroscopical qualities will depend quite on the degree of fulfilment of this condition. This fact explains the reason why inertia matrix is a very important input parameter, requiring careful evaluation. An easy and efficient method to do this provides for the use of a threedimensional CAD, which is to be equipped with a volumes calculation module: by assuming the geometrical parameters and the airfoil shape it is possible to build a mock-up, to which assign a material, that is, the density, and therefore the weight. The inertia matrix strictly depends from the swept angle, as stated above, and the research of the best configuration is reduced to a series of subsequent attempts, accomplished by acting on different parameters, such as the eccentricity (thus the swept angle), the aspect ratio, the tapering

or a possible dihedral angle. This problem is avoidable with other kinds of boomerangs, as the matter of fact other configurations like the three-blade or the X (or cross) shape, being geometrically symmetric, are more similar to a real gyroscope and are notoriously more stable in flight.

The results presented in this work are referred to a mock-up obtained through a CATIA * modalization. A medium-sized boomerang has been chosen, and a material of unitary density has been selected (it might be a seasoned or pressed wood); the geometrical and inertial parameters are summarized in the table 1.

R	0.3 m
<i>Chord</i>	0.05 m (constant)
<i>Swept Angle</i>	56.2°
<i>Diehdral Angle</i>	0°
\overline{FG}	0.0887 m
<i>Mass</i>	0.1308 Kg
J_{xx}	$2.25339e^{-3} \text{ kg m}^2$
J_{yy}	$3.44756e^{-4} \text{ kg m}^2$
J_{zz}	$2.59743e^{-3} \text{ kg m}^2$
J_{xy}	$4.1587e^{-5} \text{ kg m}^2$
J_{xz}	$-3.5184e^{-6} \text{ kg m}^2$
J_{yz}	$-6.255e^{-8} \text{ kg m}^2$

Table 1

Mathematical model:
equation of motion of a gyroscopic system

We adopt the rigid body model: this implies that the equations of motion can be decoupled into rotational equations and translational equations if, as it is, the body reference frame \mathcal{F}_B origin is chosen to be at the center of mass. Therefore the state model used is a 6-DOF model. Furthermore we adopt the NED (North-East-Down) frame on the surface of the Earth as an inertial reference frame \mathcal{F}_I . This frame is both accelerating and rotating; however the accelerations associated with the Earth's rate are negligible compared to the accelerations that can be produced by the boomerang. The flat-Earth model is also acceptable. The body reference frame \mathcal{F}_B is solid with the rotor, which means that \mathcal{F}_B is a rotating frame. This might seem a complication of the model, but actually it is the only way to follow the motion of the boomerang step by step without changing the inertia matrix, that is a full matrix:

$$J = \begin{bmatrix} J_{xx} & -J_{xy} & -J_{xz} \\ -J_{xy} & J_{yy} & -J_{yz} \\ -J_{xz} & -J_{yz} & J_{zz} \end{bmatrix} \quad (1)$$

*By IBM and Dassault

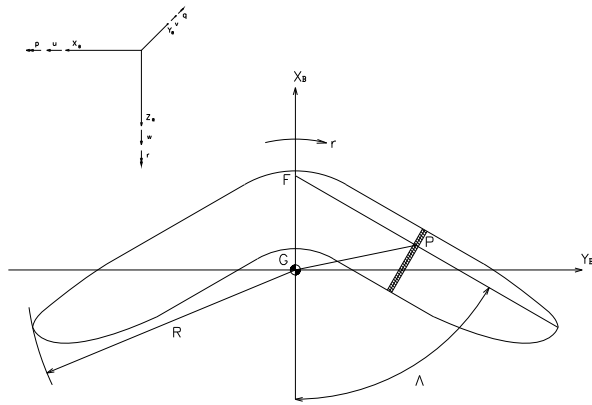


Figure 1: Reference frames

The boomerang is treated, in every respect, as a spinning rotor. Thus the most suitable way to describe its orientation in space (with respect to the inertial frame \mathcal{F}_I) is through the Euler parameters $\mathbf{q} = (q_0 \ q_1 \ q_2 \ q_3)^T$ in the form of the so-called *quaternion* four variable representation. It has been preferred to the Eulerian angles one in order to avoid the mathematical singularity that might arise in the attitude equation, where the Euler angles are bound to the angular rates p , q and r through trigonometrical (i.e. non linear) relationships. It is always possible to pass from quaternion parameters to Euler angles and vice versa, through very simple relationships, with the further advantage that the quaternion representation allows to use a linear (vectorial) attitude equation. However it has been observed that the state equations with quaternion attitude propagation are not minimal, that is quaternion parameters are not independent, but satisfy the following constraint equation:

$$\mathbf{q}^T \mathbf{q} = q_0^2 + q_1^2 + q_2^2 + q_3^2 = 1 \quad (2)$$

In simulation problems the nonminimality condition does not lead to any inconvenience, but greater care is to be used when stability and control problems are involved, because a non minimal model introduces extra modes beside the natural ones: they are simply artifacts of the method of computations and are not readily associated with real aircraft behavior.

Under those hypothesis the equations describing the boomerang motion, in the state-space formulation, are:

$$\begin{aligned} \dot{\mathbf{v}}_B &= -\tilde{\omega}_B \mathbf{v}_B + B_B \mathbf{g}_0 + \frac{\mathbf{F}_B}{m} && \text{(force eq.)} \\ \dot{\omega}_B &= -J^{-1} \tilde{\omega}_B J \omega_B + J^{-1} \mathbf{T}_B && \text{(moment eq.)} \\ \dot{\mathbf{q}} &= -\frac{1}{2} \Omega_q \mathbf{q} && \text{(attitude eq.)} \\ \dot{\mathbf{p}}_{NED} &= B_B^T \mathbf{v}_B && \text{(navigation eq.)} \end{aligned}$$

in which

$$\tilde{\omega}_B = \begin{bmatrix} 0 & -r & q \\ r & 0 & -p \\ -q & p & 0 \end{bmatrix} \quad (3)$$

$$\Omega_q = \begin{bmatrix} 0 & p & q & r \\ -p & 0 & -r & q \\ -q & r & 0 & -p \\ -r & -q & p & 0 \end{bmatrix} \quad (4)$$

\mathbf{F}_B and \mathbf{T}_B are the aerodynamical forces and moments, while B_B is the rotation matrix from NED frame to body frame, expressed in function of quaternions. In the narrow form we write

$$\dot{\mathbf{X}} = \mathbf{f}(\mathbf{X}, \mathbf{X}_0) \quad (5)$$

in which

$$\mathbf{X}^T = [\mathbf{v}_B^T, \omega_B^T, \mathbf{q}^T, \mathbf{p}_{NED}^T] \quad (6)$$

is the state vector made by a set of variable that completely define the state of the system.

In presence of local wind we assume that the wind velocity vector, that is an input of the problem, is constant over a region much larger than the size of the body; the velocity of the body centre of gravity with respect to the air is given by

$$\mathbf{v}_R = \mathbf{v}_B - B_B \begin{bmatrix} W_N \\ W_E \\ W_D \end{bmatrix} \quad (7)$$

Basis of rotor modelling

The most interesting aspect of this simulation problem is the calculation of the aerodynamical actions: we know that the aerodynamical behaviours of the boomerang is similar to that of a two-blade rotor constituted by high-efficiency airfoils fitted at a nearly null angle. During the first part of its trajectory, this rotor works in helicopter mode, that is, it produces the lift required to support the body by accelerating the air mass which passes through the rotor disk in a direction opposite to the lift direction. The rotor is said to be active. If the boomerang is a good one, the second part of the trajectory (return) takes place with the rotor in self-rotation mode: once the rotation kinetic energy given by the thrower has exhausted itself, the boomerang transforms its potential energy into rotation kinetic energy produced by the aerodynamical forces, which during this phase are driving ones; in this case the rotor is said passive. In self-rotation mode, the direction of the induced velocity is inverted, that is, a transition takes place between the two phases. Apart from this macroscopic aspect, another consideration is to

be done: boomerang flight is a phenomenon limited in time, that is, a complete time history can be performed in a few seconds, during which motion variables undergo very strong variations. This is to say that there is a frequency, associated with motion, that will obviously be compared with the natural time of evolution of physical phenomena: the higher is the motion frequency, the less time the field has to develop itself and to reach the new operating conditions and the stronger the non-stationary effects. Thus, to perform a good simulations it is necessary to use a 'sensitive' (dynamical) model.

Rotor theory has many examples of attempts of modelization, but every method has the same basic idea: to concentrate the problem on the determination of the distribution of induced velocities, that is to say that the determination of the induced velocities is at the heart of the rotor aerodynamics. Different methods have different philosophy, but it is possible to outline the state of the art as follow:

- *Vortex wake theory*: the blade is substituted by a vortex distribution, merely divided in tip vortex and an inboard vortex sheet. The trailed and shed vorticity of the rotor wake is deposited in the flow field as the blade rotates, and then convected with the local velocity of the fluid. This velocity consists of the free stream velocity and the wake self-induced velocity, so that the wake acquires the shape of distorted interlocking helices, skewed in the direction of motion. This point of view is the most exhaustive because it permits to evaluate many fluid dynamic phenomena of great importance, like the blade-vortex interaction, the self-induced distorsion, the stall of the retracting blade and many other that are not yet well understood even for non rotating wing. Nevertheless the limitations imposed by this method are quite heavy: good results are obtained only with a detailed description of the rotor geometry, including in it even the actual position of each vortex element. This justifies the birth of different level of approximation sub-methods that go from the rigid wake model (or prescribed wake model, when measured wake geometry information is used), to the free (or semirigid) wake model, through a great deployment of forces that has lead to significant results. Among all the most important is the evaluation of the flow near the rotor and the mapping of data in chart form or in look-up tables form ^[4], for various geometrical characteristics and OGE operating conditions of the rotor. These are needed for rapid calculations in flight dynamics and control simulations, when it is necessary to estimate efficiently the effects of the interactions

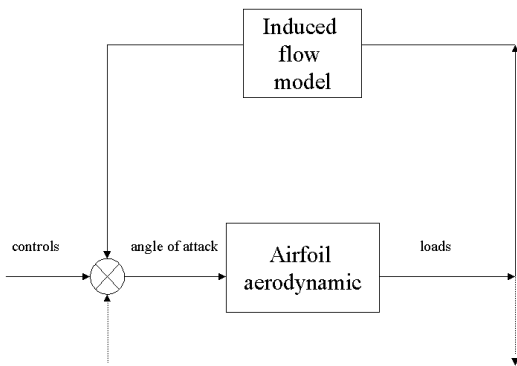


Figure 2: inflow dynamic as a closed-loop problem

between the rotor(s) and the body (helicopter fuselage).

- *Dynamic inflow theory*: inflow is treated globally, as a large mass of air accelerating through the rotor disk, in function of the radial and azimuthal position, as stated in the following first harmonic relation

$$v_i = v_0 + v_{i_c} \frac{r}{R} \cos \psi + v_{i_s} \frac{r}{R} \sin \psi \quad (8)$$

This method was initiated by Curtis and Shupe in 1970: they opened a great seam of research inheriting from Sissingh his quasi-steady formulation, that did not take into account the radial variation of the inflow, the time lag and the flow perturbations in pitch and roll moments. Since the 1980's, dynamic inflow has been one of the most investigated areas of research. Nowadays it seems to have given some satisfaction: the Pitt-Peters model seems to be quite reliable, complete and easy to use, but other work is to be done to give it a numerical (experimental) validation, beyond the methodological one. The formulation of the Pitt-Peters model will be outlined in the next section.

I am very far from thinking to have well resumed the subject; from this point of view there are few authoritative and very precious works, among all the one by R.T. Chen ^[5] and the more targeted one by G.H. Gaonkar and D.A. Peters ^[6]. Nevertheless there is a concept to underline: dynamic inflow is intrinsically a closed-loop problem, as shown in figure 2 for the general case of a controlled machine (helicopter), but Pitt-Peters model treats it as an open-loop problem, reducing time calculation without losing its own generality.

Each phase of boomerang flight has been simulated: first of all the throwing one, that represents the *constrained motion phase*. Some words must be spent on it, even if it is not interesting from the aeronautical point of view. One can imagine a throwing machine, constituted by a mechanical arm, lying on a plane which is orientable with respect to the NED frame. In correspondence of one tip of the arm there is the hooking-unhooking boomerang mechanism, on the other side the arm is bound to the plane through a cylindrical torsional spring: it is possible to set the starting and the ending points of the run of the arm and calculate the elastic moment that the arm is subjected to, with the following linear relationship:

$$M = \Delta\varphi \frac{G d^4}{32 n D} \quad (9)$$

where $\Delta\varphi$ is the azimuthal variation of the arm position, d and n are, respectively, the diameter and the number of the coils, D the diameter of the spring, and G is the elastic torsional coefficient. The motion of the arm is planar and is described by three second order scalar equations, which are integrated instant by instant up to the unhooking moment. The virtual (simulated) thrower-machine is used with the aim of calculating the state vector, and its derivative, proper of the first instant of the *free motion phase* (that coincides with the last instant of the constrained motion phase). Even the real one is useful: the simulated trajectories can be compared to the actual ones of a numerical-control model, constituted ad hoc by the very same airfoils used in the test case model (airfoils whose aerodynamical characteristics are obviously known). In this way it is possible to validate the mathematical model, being sure to have imposed the right initial conditions.

During the constrained phase, the aerodynamical forces and moments have been neglected. This is not a roughly approximation and we can prove it if we compare the inertial end elastic forces with some hypothetical values that the aerodynamical forces would have, if they were evaluated in steady condition. Furthermore this phase wears out in few split seconds, so that accelerations acquire the impulsive characteristic; aerodynamical forces have not enough time to develop themselves and reach a value that is even half the steady one (let us remember the case of the impulsive start of the plate, studied by H. Wagner ^[7] in 1925). The flight initial state vector is then the result of the balance among inertial, elastic and gravitational actions. In order to have good flight performances much power is to be impressed to the boomerang: it is literally hurled by the thrower

and undergoes great tangential and centrifugal accelerations, whose actions will influence the whole trajectory [†], as will be pointed out in the section regarding the discussion of the results.

As soon as the free motion phase starts, the aerodynamical actions, and their variations in time, begin to play an important role. To perform the simulation, the nonlinear version of the Pitt-Peters dynamic inflow model has been used. It consists in a first-order differential vectorial nondimensional equation to be added to the above mentioned state equations [‡]:

$$\begin{bmatrix} \dot{\lambda}_0 \\ \dot{\lambda}_s \\ \dot{\lambda}_c \end{bmatrix} = -[M]^{-1} [V] [\mathcal{L}]^{-1} \begin{bmatrix} \lambda_0 \\ \lambda_s \\ \lambda_c \end{bmatrix} + [M]^{-1} \begin{bmatrix} C_T \\ C_1 \\ -C_2 \end{bmatrix} \quad (10) \quad \text{aero}$$

in which

$$[\lambda] = \begin{bmatrix} \lambda_0 \\ \lambda_s \\ \lambda_c \end{bmatrix} \quad (11)$$

is the nondimensional induced velocity vector in body axis, while C_T , C_1 and C_2 are, respectively, the thrust, the rolling moment and the pitching moment coefficients, in body axis [§]. This explicit formulation is derived from the most famous implicit one, nondimensional, written in a general coordinate system, that is worth quoting:

$$[M] \begin{bmatrix} \dot{\lambda}_0 \\ \dot{\lambda}_s \\ \dot{\lambda}_c \end{bmatrix} + [L]_{nl}^{-1} \begin{bmatrix} \lambda_0 \\ \lambda_s \\ \lambda_c \end{bmatrix} = \begin{bmatrix} C_T \\ -C_L \\ -C_M \end{bmatrix} \quad (12) \quad \text{aero}$$

The transformation between the two formulations is well explained by the same author of the theory in a technical note ^[8], in which some aspects of the model are reviewed and corrected for practical applications. Essentially it is the rewrite of the model in a more usable form, that is from a generic reference frame, to a body reference frame. For further details the reader is invited to look over the work by Peters and HaQuang. The general formulation, however, is useful because allows to have a greater insight into the range of applicability of this theory. The $[M]$ matrix, for example, is nothing more that

[†]Here *trajectory* has its wider meaning: it is the points locus described by the state vector tip, instant by instant, in the phase space.

[‡]note that, before application, each term is to be switched to its dimensional form, and, above all, great care is to be taken when nondimensional equations are integrated together with the dimensional ones, because in the former case time is normalized on the rotor speed.

[§]The subscript *aero* implies that only aerodynamic contributions are considered in C_T , C_L and C_M . For this application this detail is meaningless, because inertial terms due to flapping or lagging blades are absent. Anyway the author has reported it for completeness.

an inertial term, that allows to include the effects of the time delay in the build-up or decay of the inflow field. It is called *apparent mass matrix*; the problem of its evaluation has been the subject matter of extensive studies, first by Carpenter and Fridovitch, in 1953, who introduced the intuitive concept of the rotor seen as an impermeable disk which, under the actions of instantaneous acceleration and rotation in still air, produces reactions forces. They suggested that the transient inflow through the rotor, in axial flight, could be taken into account by including an accelerating mass of air occupying 63.7% of the air mass of the circumscribed sphere of the rotor:

$$m_S = \frac{4}{3}\pi\rho R^3$$

$$m_A = \frac{8}{3}\rho R^3 \cong 0.637 m_S \quad (13)$$

$$m_{11} = \frac{m_A}{\pi\rho R^3} = \frac{8}{3\pi}$$

A similar concept was applied to the apparent inertia, that was estimated to be a certain percentage of the rotary inertia of the same sphere. Therefore we have:

$$[M] = \begin{bmatrix} \frac{8}{3\pi} & 0 & 0 \\ 0 & \frac{16}{45\pi} & 0 \\ 0 & 0 & \frac{16}{45\pi} \end{bmatrix} \quad (14)$$

What seems to be a fanciful idea was confirmed both by experimental tests, and by the analytical study by Pitt and Peters ^[9]. This latter is quite interesting and allows us to arrive at the focus point: the development of this model is based on an extension of the actuator-disc theory and this means that no geometrical parameters are involved in the determination of matrix coefficients. It does not matter how many blades the rotor has, or what their shape is and, moreover, adopting the first-harmonic form of the model, as we did, even the pressure distribution is little influential on the matrix coefficients.

Similar deductions are valid also in the case of the $[L]_{nl}$ matrix. It is function of the wake angle α (measured with respect to the rotor disk) and of the mass-flow parameter matrix $[V]$, that weighs the mass-flow relatively to the associated action:

$$[L]_{nl} = [L][V]^{-1} \quad (15)$$

$$[L] = \begin{bmatrix} \frac{1}{2} & 0 & -\frac{15\pi}{64} \sqrt{\frac{1-\sin\alpha}{1+\sin\alpha}} \\ 0 & \frac{4}{1+\sin\alpha} & 0 \\ \frac{15\pi}{64} \sqrt{\frac{1-\sin\alpha}{1+\sin\alpha}} & 0 & \frac{4\sin\alpha}{1+\sin\alpha} \end{bmatrix} \quad (16)$$

$$[V] = \begin{bmatrix} V_T & 0 & 0 \\ 0 & V & 0 \\ 0 & 0 & V \end{bmatrix} \quad (17)$$

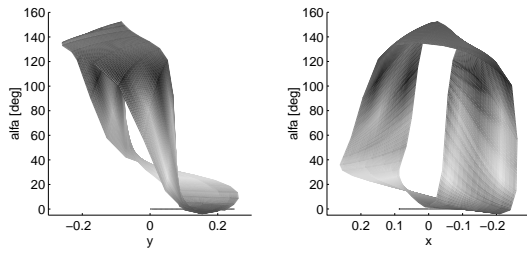


Figure 3: angles of attack of the advancing blade ($time = 0.525\ sec$)

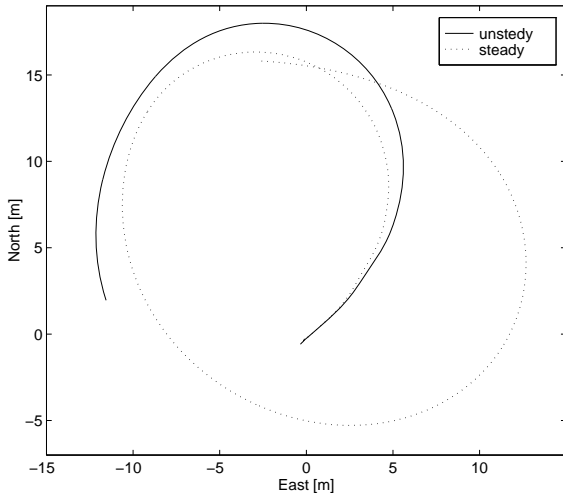


Figure 4: comparison between the steady and the unsteady model (1)

$$TA_{st} = 7.125\ sec$$

$$TA_{unst} = 2.445\ sec$$

This apparent digression is at the base of the remarks that, in some manner, justifies the application of a model, developed for helicopter rotors, to a very particular rotor, that is, an eccentric one. We conclude by observing that boomerang flight is performed at very high values of the advancing ratio, when the induced velocities are nearly negligible with respect to the inflow due to forward motion. Notwithstanding this, their variations with time (unsteady effects) are consistent and this dynamic inflow model has demonstrated to be a good evaluation tool, as will be shown below.

The aerodynamical actions have been evaluated by using the blade-element theory: forces and moments are calculated by the superpositions of the contributions of each blade section, that is supposed

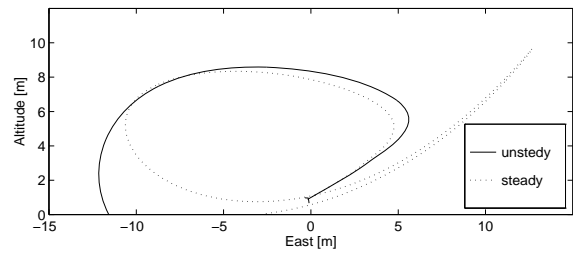


Figure 5: comparison between the steady and the unsteady model (2)

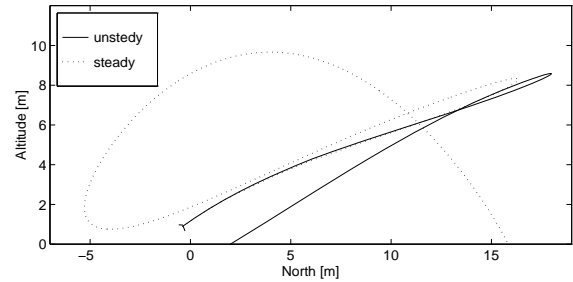


Figure 6: comparison between the steady and the unsteady model (3)

to have the same characteristics of its constituting airfoil. Each elementary action has been evaluated by knowing the velocity components of the air relative to any point, thus the local angle of attack, and by interpolating the data extracted from the known airfoil characteristic curves. The elementary actions then have been numerically integrated along the blade: this procedure is repeated every time that the state vector derivative is calculated, that is four times per step, if an RK4 integration routine is used. This method is expensive, in time-calculation terms, but it may happen to be very far from linear conditions, above all where the blade is retreating and thus where wind blows from the trailing-edge. At very high advancing ratio values, this reverse-flow region may be wide and a reliable evaluation of the aerodynamical actions might be impossible by using the analytical integration (that is by assuming a constant lift slope and so on...). The choice of the airfoil has fallen on a wind-turbin one, the Wortmann FX84-W-127, whose characteristics have been experimentally evaluated some years ago at the Polytechnic of Turin ^[12]. It has demonstrated to be very suited for this application, due to its good autorotative qualities, that are required for the boomerang as well as for wind-turbin. Figures 8 and 9 show how rotational speed increases considerably, symptom that the boomerang is little braked during its rotation; this allows for a very slow final descent, as shown in figure 8.

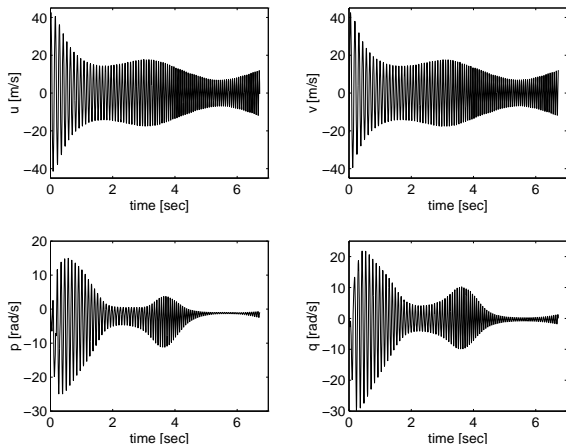


Figure 7: components of the translational and rotational speed along the x_B and y_B axis
 $TA = 6.725 \text{ sec}$

The mathematical system constituted by the thirteen state equations and the three inflow equations 10 has been integrated in time with an RK4 routine. The choice of the integration algorithm has been made by trying to match the philosophy of the space-state formulation adopted, in which all the information describing the state of the system is contained in the state vector \mathbf{X} at any given instant: the RK method, unlike the multistep ones, allows to solve the initial value problem apart from the past values. The sample time has been chosen in function of the rotational speed r : it has been reduced until its further halving has demonstrated to be influential on the results. r varies during the motion, it can even double, so that in the simulation program an adaptative step option has been provided for.

Analysis of a flight

The mathematical system describing the physical one is nonlinear through the B_B matrix, the Ω_q matrix and the aerodynamical actions and, moreover, the degrees of freedom are coupled. Thus the time history and the stability of the system will be strongly dependent on the throwing parameters and the atmospheric conditions. The solid curves of figures 10, 11 and 12 show the geographical trajectory, in terms of NED coordinates, performed by a test boomerang, whose geometrical parameters are resumed in table 1. Figures 7, 8 and 9 are representative of the same flight and can be useful to understand the reasons of the behaviour of the boomerang. At the throw moment Euler angles are

$$\phi = -73.38^\circ \quad \theta = 52.62^\circ \quad \psi = 58.35^\circ \quad (18)$$

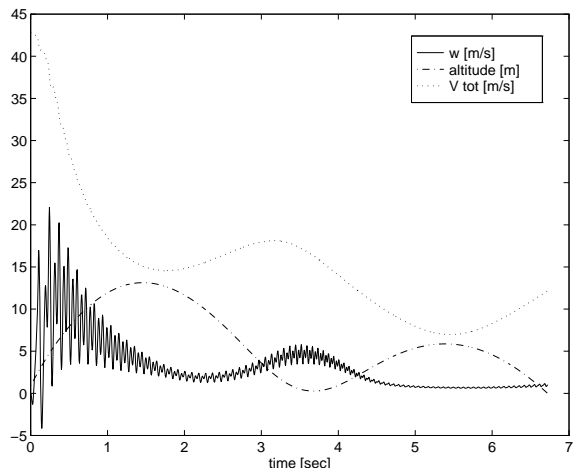


Figure 8: effect of the altitude on the amplitude modulation
 $TA = 6.725 \text{ sec}$

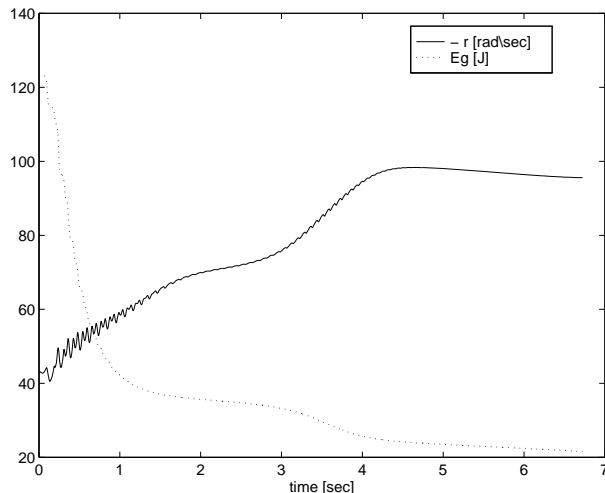


Figure 9: component of the rotational speed along the z_B axis: note that it is negative (this is consistent because the trower is supposed to be right hander). There is traced also the total energy, evaluated by adding kinetical and potential energy contributions

$TA = 6.725 \text{ sec}$

which means that the xy_B plane is nearly normal with respect to the ground and the xz_B plane has a little climbing ramp. In the first phase of the flight the system has a high translational speed that, in absence of wind, is the composition of the inplain velocities u and v . It takes off under the initial actions of great centrifugal and tangential accelerations and, as soon as aerodynamical forces become substantial, the trajectory bends and the w velocity component starts to develop. The boomerang begins its turn and, while the translational speed decreases, the rotational speed can increase, decrease or remain constant, depending on the autorotative characteristics of the system. Evidently, an increase of the rotational speed occurs to the cost of the translational one, for obvious energetic considerations: thus a highly autorotative boomerang covers little distances, because it spends a great amount of energy in whirring; but if the throw is performed with high power, the autorotative boomerang is able to complete its turn with a very slow descent, that is more spectacular as well as more precise ¶.

By analysing the surfaces representing the induced velocities, corresponding to some instants after the throw (figure 3), we see that the advancing blade is strongly loaded when its anomaly is of some degrees greater than the reference position $\psi_a = 90^\circ$ (positive y_B axis): lifting forces are concentrated there and in a much greater extent, if we think that the advancing blade has also higher effective local velocities

$$V_{eff} = \sqrt{U_P^2 + U_T^2} \quad (19)$$

where U_P is the parallel component of the local velocity, with respect to the rotor disk, while U_T is the tangential one, that strongly feels the effects of the forward speed. All this means that, on an average, that direction provides the position of the pressure centre and subsequently of the precessing axis. In fact the latter is defined as the intersection between the rotational plane and the plane that contains the couple, created by the lifting actions, applied in the pressure centre and the inertial and gravitational forces, applied in the centre of the mass. The precessing angular velocity vector, that lies on this axis, has thus both a component along the y axis and one along the x axis, so while the former is responsible of the further bending of the trajectory the latter produces the ‘flattening’ of the boomerang: the xy_B plane reduces its inclination with respect to the ground, slowly assuming a horizontal orientation. But this motion is almost imperceptible and the trajectory has the time to complete itself, before the flattening can take place. In the meantime, the

¶ this characteristic is associated with a certain form of stability, but this is an intuitive concept more than a mathematical one.

body has reached its upper point, in correspondence of which the translational speed has a local minimum. The following glide occurs under the action of the gravitational field: the boomerang descends in autorotation with a strong recovery of kinetic energy; the translational and the rotational speeds increase while the rotational plane becomes more and more horizontal. This is the reason why at a given instant, just at the end of the flight, when the body is landing, the trajectory turns to climb, because the lifting actions have assumed the z_{NED} direction. The trajectory has now accomplished a complete turn and, depending on the amount of residual power and, to much greater extent, on the presence of wind, it can end in different way: if the airfoils constituting the boomerang have high efficiency, the trajectory goes on with another turn, as long as it is allowed to by the power; it may happen that, just before the end of the turn, the rotational plane tilts to the other side and the boomerang enters in an opposite narrow turn, completing what is called ‘the eight’. In the best case, the trajectory ends in a vertical autorotation in correspondence of the geographical initial point. What determines a situation instead of another? Figures 10, 11 and 12 show the comparison between two trajectories obtained from the same initial and environmental conditions, but in one case airfoils efficiency has been decreased by an 70%, with respect to the nominal one: precisely, the values of drag coefficient have been kept constant, as the moment coefficient ones, while the c_l curve has simply undergone a contraction equivalent to 70% †. The trajectory then becomes wider and reaches higher altitudes. On the contrary, it may happen that airfoils efficiency is not satisfactory, that is, the boomerang is not able to perform its turn. In this case, experience teaches that a little positive tip incidence can be useful, but can also compromise the boomerang autorotative qualities.

Parameters influence on the trajectory

The variables of figure 7 are representative of the same flight. They show a behaviour that, in one way, reminds of a beat phenomenon: namely a sinusoid, whose frequency is imposed by the rotational speed r , modulated by a sinusoidal amplitude. The latter is strictly bound to the oscillations of the total translational speed, which, in its turn, decreases and increases according to the trend of the boomerang to climb or to descend, keeping anyway an average decreasing course. Figure 8 shows what has just been

† This method is used even in the practical situations: the boomerang is calibrated by the airfoils shape modifications to perform the desired trajectory. It means that this is a case in which the high efficiency condition is not required at all costs.

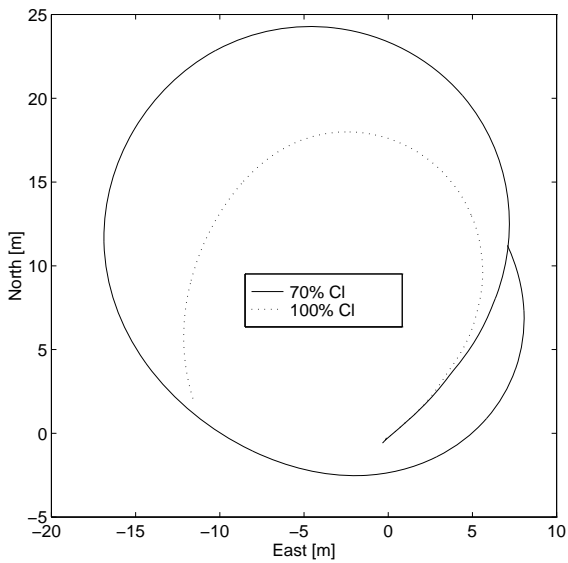


Figure 10: influence of the aerodynamical characteristics (1)

$$TA_1 = 2.445 \text{ sec}$$

$$TA_{0.7} = 6.725 \text{ sec}$$

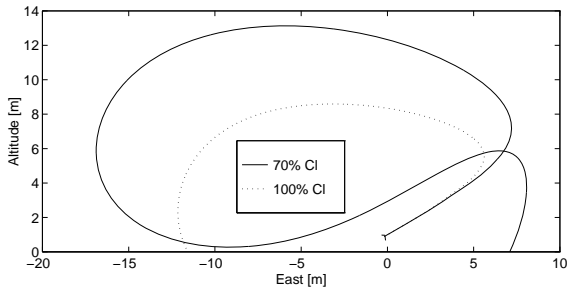


Figure 11: influence of the aerodynamical characteristics (2)

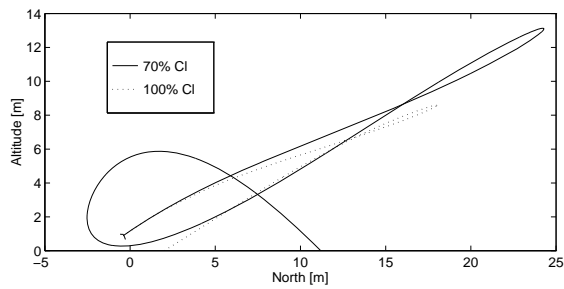


Figure 12: influence of the aerodynamical characteristics (3)

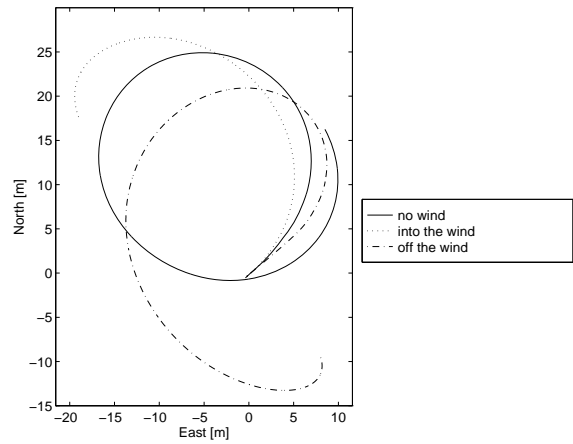


Figure 13: influence of the wind (1). A wind of 4 m/s is blowing toward north (into the wind), and from north (off the wind)

$$TA_{into} = 3.025 \text{ sec}$$

$$TA_{off} = 6.225 \text{ sec}$$

$$TA_{nw} = 6.735 \text{ sec}$$

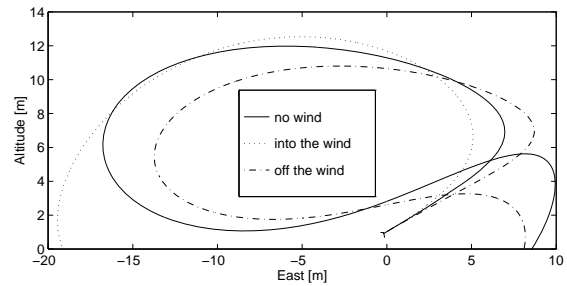


Figure 14: influence of the wind (2)

stated; being the system strongly nonlinear, the parameters of this damped beat oscillation will depend on the characteristics of the system as much as on the throwing conditions, which seem to be able to modify the system natural modes.

Figures 13, 14 and 15 show the influence of the wind: a contrary wind subtracts a greater amount of energy from the system, nevertheless the flight results longer; a favourable wind is less expensive, in terms of energy, but the boomerang is crushed to the ground in a few seconds. This trend is well known among the throwers, in fact the first rule to learn is to throw about 45° off the wind.

Figures 16, 17 and 18 show another well known behaviour: in this case the varying parameter is the angle of inclination of the xy_B plane, with respect to the xy_{NED} plane, at the throwing instant, namely the angle ϕ_P of inclination of the throwing-machine plane, with respect to the ground. The more horizontal the angle, the higher the trajectory, because

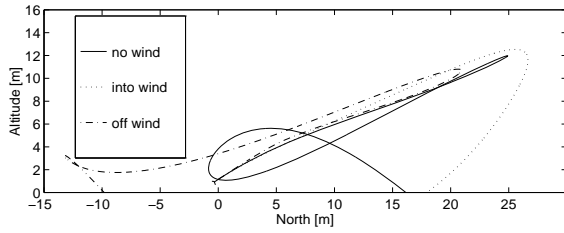


Figure 15: influence of the wind (3)

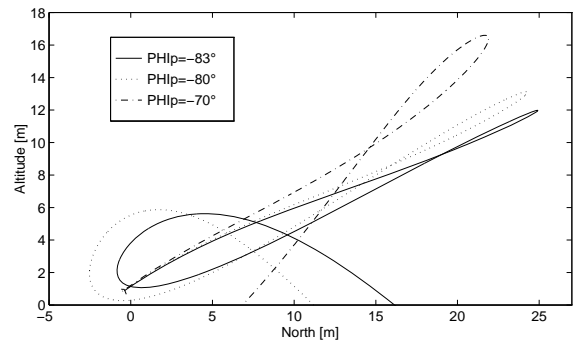


Figure 18: influence of the ϕ_P angle (3)

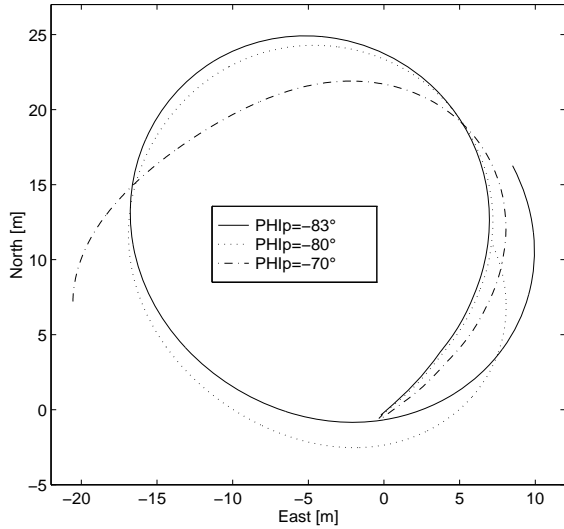


Figure 16: influence of the ϕ_P angle (1):

$$TA_{70} = 3.350 \text{ sec}$$

$$TA_{80} = 6.725 \text{ sec}$$

$$TA_{83} = 6.735 \text{ sec}$$

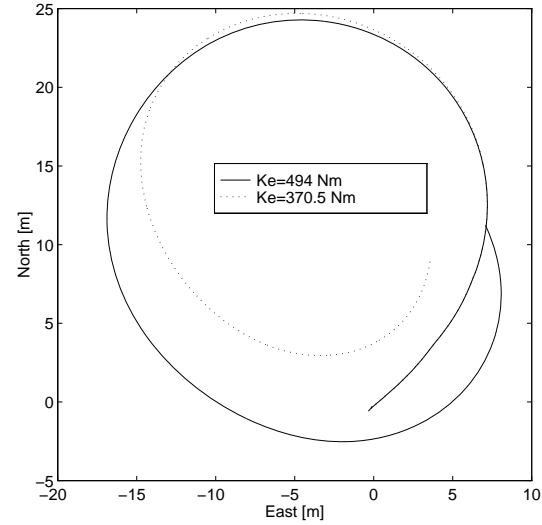


Figure 19: influence of the throw power (1). It is modified through the spring elastic constant k_e of the thrower-machine

$$TA_{494} = 6.725 \text{ sec}$$

$$TA_{370} = 6.040 \text{ sec}$$

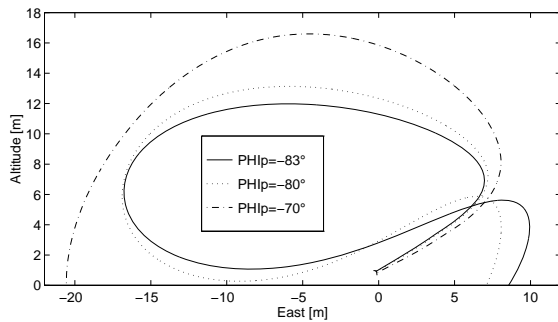


Figure 17: influence of the ϕ_P angle (2)

the lifting force has a greater component along the z_{NED} direction. To run the additional five or ten meters of altitude, the body loses rotational kinetic energy: the angular speed vector decreases and the precessing moments $\tilde{\omega} [J] \omega$ are no more able to tilt the boomerang, that crushes in a few seconds.

Figures 19, 20 and 21 show the influence of the throw power: it is modified by varying the elastic constant k_e of the spring, that produces the bending moment on the thrower-machine arm. Using a torsional spring the bending moment is linear with k_e , so that a smaller value of k_e implies a lower throwing power. Apart from the last tract, the diameter of the trajectory seems to feel no effects, while the altitude is affected. This trend has been detected and analysed also by other authors ^{[13] [15]}, who agree in

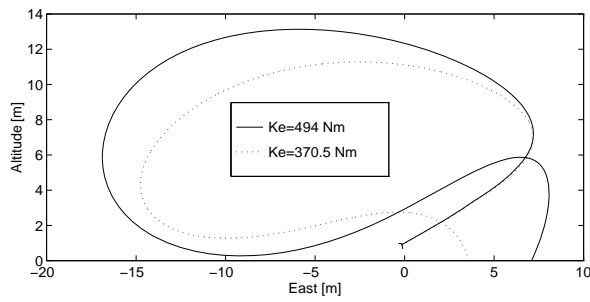


Figure 20: influence of the throw power (2)

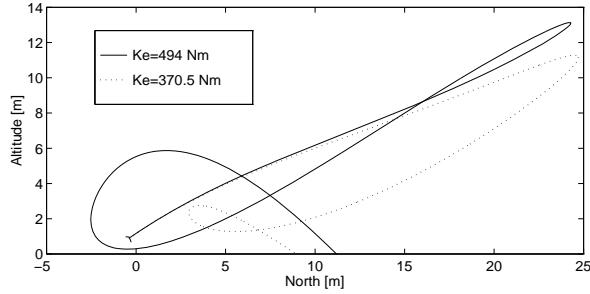


Figure 21: influence of the throw power (3)

stating that the boomerang seems to ‘possess’ its trajectory radius in itself.

In conclusion figure 4, 5 and 6 reports a comparison between two trajectories, obtained with the same throwing parameters, but in one case the unsteady effects have not been taken into account, namely the induced velocity is the one that resolves the closed-loop problem, based on the momentum theory. The differences are remarkable, above all in terms of time calculation: resolving a closed-loop problem requires a time of some orders of magnitude greater than the case of the open-loop problem. Furthermore the trajectory evaluated with the steady

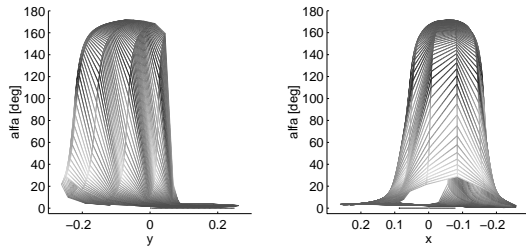


Figure 22: angles of attack of the advancing blade (*time = 2.520 sec*)

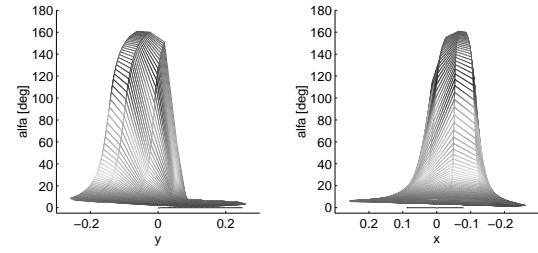


Figure 23: angles of attack of the advancing blade (*time = 4.110 sec*)

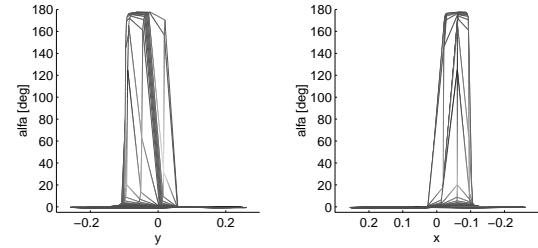


Figure 24: angles of attack of the advancing blade (*time = 5.030 sec*)

model has clearly something unnatural and, in fact, has never been verified experimentally.

Topographical analysis of the angle of attack

Figures 3, 22, 23 and 24 are quite interesting: they show the topographical situation of the angles of attack of the advancing blade, in four different phases of the motion. They have been traced by mapping, instant by instant, the whole turn of the advancing blade, erasing the central part that is meaningless, as it corresponds to a pressure hole (but it is of no easy interpretation, in fact this area would not be swept by the blades, if the body had not a forward motion). It is easy to see that the reverse flow region narrows during the flight: this is perfectly coherent, in fact the local angle of attack is due to the superposition of an increasing rotational speed r and a decreasing total translational one. At the end of the flight the rotational speed is very high, so that it prevails over the translational one and the reverse flow region disappears.

Conclusions

The results that have been presented show that this simulation program is able to treat strongly unsteady motions, such as the boomerang flight. The boomerang is seen as a rotor working at very high advancing ratio; no geometrical limitation is imposed, so that boomerang behaviours of different shapes and dimensions can be compared, under any environmental condition. Usteady effects, which are predominant during the whole flight, are well treated by the Pitt-Peters dynamic inflow model. The latter is based on the resolution of an open-loop program, unlike other models, so that a whole flight (that takes some seconds) can be simulated in a few tens of minutes. This application can be interesting as the boomerang is a truly free rotor with a known, or easy to experiment, behaviour, thus representing a good means to verify the reliability of any numerical code, written, for example, for helicopter applications.

List of Symbols

\mathbf{X}	state vector
$\mathbf{v}_B^T = (u, v, w)$	linear velocity vector of the system's center of gravity (in absence of wind)
\mathbf{v}_R	linear velocity vector of the system's center of gravity in presence of wind
$\omega_B^T = (p, q, r)$	rotational velocity vector of the system in body axes
$\Phi^T = (\varphi, \theta, \psi)$	Euler angles
$\mathbf{q}^T = (q_0, q_1, q_2, q_3)$	quaternions
$\mathbf{p}_{NED}^T = (N, E, h)$	coordinates with respect to the NED inertial system
$\mathbf{F}_B^T = (X, Y, Z)$	vector of forces in body axes
\mathbf{F}_{AB}	vector of aerodynamic forces (in body axes)
$\mathbf{T}_B^T = (l, m, n)$	vector of moments in body axes
\mathbf{T}_{AB}	vector of aerodynamic moments (in body axes)
\mathbf{g}	gravity acceleration vector
J	inertia matrix
B_B	rotation matrix (from \mathcal{F}_I to \mathcal{F}_B)
$\lambda^T = (\lambda_0, \lambda_s, \lambda_c)$	induced velocities vector
k_e	spring elastic constant
TA	time aloft

References

- [1] BRIAN L. STEVENS, FRANK L. LEWIS
Aircraft Control Simulation
(John Wiley & Sons, New York, 1992).
- [2] GARETH D. PADFIELD
Helicopter Flight Dynamics
(Blackwell Science, 1996).
- [3] A. R. S. BRAMWELL
Helicopter Dynamics
(Edward Arnold, London, 1976).

- [4] J. W. JR JEWEL, H. H. HEYSON
Induced Velocities Near a Lifting Rotor with Nonuniform Disk Loading
(NACA Rept.1319, 1957).
- [5] ROBERT T. N. CHEN
A Survey of Nonuniform Inflow Models for Rotorcraft Flight Dynamics and Control Applications
(Vertica, vol. 14 n. 2, Great Britain, 1990).
- [6] G. H. GAONKAR, D. A. PETERS
Review of Dynamic Inflow Modeling for Rotorcraft Flight Dynamics
(Vertica, vol. 12 n. 3, Great Britain, 1988).
- [7] H. WAGNER
Über die Entstehung des dynamischen Auftriebes von Tragflügeln
(ZAMM, 1925).
- [8] DAVID A. PETERS, NINH HAQUANG
Dynamic Inflow for Practical Applications
(Journal of American Helicopter Society, October 1988).
- [9] DALE M. PITT, DAVID A. PETERS
Theoretical Prediction of Dynamic-Inflow Derivatives
(Vertica, Vol. 5, Great Britain, 1981).
- [10] B. ETKIN
Dynamics of Atmospheric Flight
(John Wiley & Sons, Toronto, 1972).
- [11] D. GRAHAM, D. McRUER
Analysis of Nonlinear Control System
(John Wiley & Sons, New York, 1961).
- [12] S. D'ANGELO, P.GILI
Wind Tunnel Measurements of Aerodynamic Coefficients of Asymmetrical Airfoil Sections for Wind Turbin Blades Extended to High Angle of Attack
(Wind Energy R&D Programme, Bruxelles, 23/24 November 1987).
- [13] GIACOMO AUGUSTO PIGNONE
Boomerang: fascino di un'arma preistorica
(Editoriale Olimpia, Italy, 1986).
- [14] MICHAEL VALENTI
The return of the boomerang
(Mechanical Engineering, December 1993).
- [15] FELIX HESS
L'aerodinamica del boomerang
(Le Scienze, April 1969).